Progress In Electromagnetics Research C, Vol. 130, 69–82, 2023

Pressure Sensing Based on Photonic Crystal Fiber by Infiltrating the Air-Holes with Water

Ilhem Mired[1, 2, *], Mohammed Debbal[2, 3], and Hicham Chikh-Bled[3, 4]

Abstract—Photonic crystal fiber sensors could be used for a variety of purposes including food preservation, manufacturing, biomedicine, and environmental monitoring. These sensors work based on novel and adaptable photonic crystal fiber (PCF) structures, and controlled light propagation for the measurement of amplitude, phase, polarization, the wavelength of the spectrum and PCF incorporated interferometry techniques. A new design of PCF was presented in this paper, and a hexagonal microstructured fiber structure was designed. The proposed PCF can successfully compensate for the chromatic dispersion by the influence of the pressure. As a result, a PCF pressure sensor was then successfully developed. The pressure sensitivity of this PCF was measured. We developed a simulation to understand the relationship between pressure and dispersion. In this work, all simulations are discussed, and the pressure sensitivity was numerically calculated for three wavelengths 1.1 μm, 1.4 μm and 1.7 μm to be respectively −0.01 (ps/nm/km)/bar 0.0207737 (ps/nm/km)/bar and 0.0236908 (ps/nm/km)/bar.

1. INTRODUCTION

In recent decades, photonic crystals have been developed into interesting new light-control and light-manipulation structures. The periodic microstructures known as photonic crystal fibers (PCFs) are those in which the refractive indexes of the materials change in one, two, or three directions over time, with a period in order of the optical wavelength [1]. A single substance, such as silica, is used to create PCFs, which have microscopic airholes along the length of the fiber. Russell's group initially used the term "photonic crystal fiber" in the early 1990s [2]. PCF is a type of fiber that overcomes the limitations of conventional optics and offers new and improved properties fiber. These limitations are related to its geometry and refractive index profile which does not allow for freely engineering optical fiber features such as inherent losses, dispersion, nonlinearity, and birefringence in order to advance in applications such as sensors. Due to its form, the length of the fiber is perforated with an irregular array of air holes. First, a hexagonal photonic crystal fiber structure was designed. To attain appropriate guiding properties, novel structures like triangular [3], circular [4], square [5], octagonal [6], hybrid [7], decagonal [8], and hexagonal PCFs [9] have been developed over time as a result of advancements in manufacturing technology. Topaz [10], Teflon [11], tellurite [12], silica [13], and other substances have all been employed to enhance the functionality of photonic crystal fiber architecture. As a result, with advances in fabrication technology, low bending loss [14], high sensitivity [15], high numerical aperture [16], high nonlinearity [17], wide mode area [18], strong birefringence [19], ultra-flat-top dispersion [20], zero-flat dispersion [21], and low inclusion loss [22] are all characteristics of PCFs [23]. PCF design is very flexible. In Fig. 1(b), numerous parameters are shown for manipulation, including the refractive index of the glass, the lattice pitch "Λ", the air hole form and diameter "d", the lattice

Received 25 December 2022, Accepted 3 February 2023, Scheduled 21 February 2023
* Corresponding author: Ilhem Mired (miredilhem.l2@gmail.com).
[1] Smart Structure Laboratory (SLL). [2] Belhadj BOUCHAIB University, 46000 Ain-Temouchent, Algeria. [3] Telecommunications Laboratory of Tlemcen (LTT), Tlemcen 13000, Algeria. [4] Abou-Bekr BELKAID University, Tlemcen 13000, Algeria.

type, and more. The design freedom makes it possible to obtain endless single-mode fibers [24] that are single-mode in the entire optical region and have no cutoff wavelength. Additionally, PCF has two guidance mechanisms. The first is the index guidance mechanism [25] (similar to conventional optical fibers) as shown in Fig. 1(a), and the second is the photonic bandgap mechanism [26].

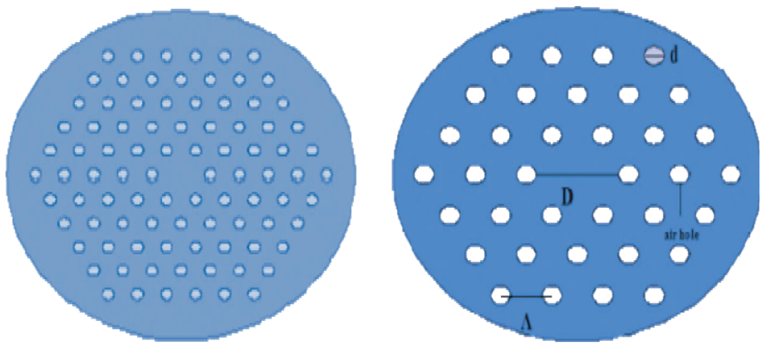

(a) (b)

Figure 1. (a) Index-guided fiber. (b) Cross-section of a PCF [23].

The modification of a variety of characteristics, including the refractive index of fibers, airhole constant, and periodic arrangement of airholes (also known as hollow channels), can achieve different applications of desirable optical properties that are studied such as birefringence, anomalous dispersion, and non-linearity [27]. For the general public, using optical fibers for communications is now an established practice. More than a century ago, these technologies were created for this market. New measurement techniques based on fiber optics have also been made possible by broad use [28]. Numerous benefits of fiber-optic sensors include their inherent immunity to electromagnetic fields (micro-waves, radio frequencies, high-energy magnetic fields, etc.. . .) [29]. Then, because of their strength and thermal or chemical resistance, they may be used in the petroleum [30], aerospace [31] nuclear industries [32], agro-food engineering [33], civil engineering [34]. . .

Currently, the world of fiber optic sensors is growing rapidly, and their use is becoming more widespread, although their development and use are only just beginning to be standardized [35]. PCFs have a variety of characteristics [36, 37] being coupled to detecting applications such as temperature independent strain sensors, which are common to regular filaments [38, 39]. The well-known refractive index exchange phenomenon, which guarantees regulated light transmission in dielectric or semiconducting materials, is frequently the basis for the operation of such devices.

The technology based on this effect has been in use for a long time and has now reached the physical performance limits [40]. Research into new materials has only recently opened up a whole new class of photonic bandgap effects [41]. This discovery sparked great interest in photonic crystals, a new class of materials that exploit the bandgap fiber (PBG) effect. It is expected to have a significant impact on multiple photonics applications [42].

A fiber sensor is generally sensitive to several physical quantities, of which pressure is often one. Therefore, our main goal was to find devices that are exclusively sensitive to one parameter and unaffected by the effects of the others. Due to their low cost, high sensitivity, small size, robustness, flexibility, and capability for remote monitoring, fiber optic sensors are an attractive option for the electronics industry [43, 44]. Other benefits support their suitability for usage even in difficult conditions including noise, strong electromagnetic fields, high voltage, nuclear radiation, and situations that are explosive or chemically corrosive [45, 46]. However, despite their excellent performance, the intrinsic properties of silica impose restrictions on the development of this technology [47]. The first, and most obvious, is the selection of the core and cladding material. Other restrictions are geometry and refractive index profile, which prevent free engineering of its characteristics such as inherent material losses, dispersion, non-linearity, and birefringence [48, 49]. Another notable feature of these PCF-based sensors, when being employed as pressure sensors is their minimal temperature sensitivity [50].

Recently, using Polarization-Maintaining Photonics Crystal Fibers (PM-PCF) as the sensing element, a novel fiber Sagnac interferometer pressure sensor has been proposed and tested [51]. By using a pressure-assisted CO_2 laser beam-scanning technology to periodically inflate airholes of the PCF, it successfully shows a unique PCF for high-sensitivity gas pressure measurement [52]. Using the polarization-maintaining PCF PM-1550-01 produced by Blaze Photonics, a PCF pressure sensor shown in Fig. 2 has been created successfully [42]. With the aid of a PM PCF-based Sagnac interferometer, the potential of a high-pressure sensor for downhole use has been shown [53]. It has been reported that Tapered Long-Period fiber-optic Gratings (TLPGs) have been used to build a tiny reflecting form of fiber-optic pressure sensor [54].

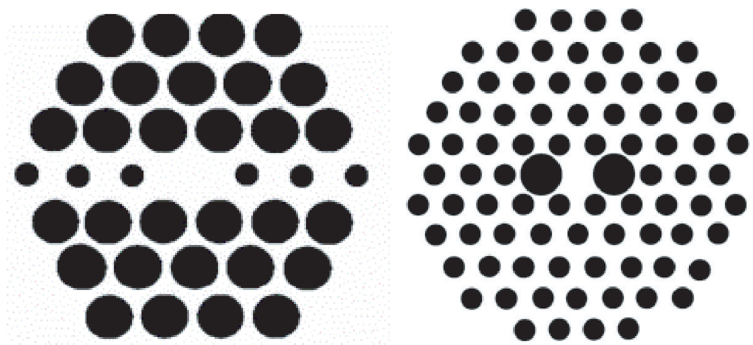

Figure 2. Cross section of a PCF sensor of pressure [42]. (a) PCF modeled by manufactured by Thermo-Electric Generators (TEGS) Inc. (b) PCF made of a commercially available Blaze photonics PCF, PM-1550-01.

The problem is to measure pressure in different environments, and as normal sensors do not give such accuracy, our contribution is to use photonic crystal fibers with a diameter of 125 µm. To show that pressure could influence the chromatic dispersion of PCFs the main objective is to develop new functional principles for fiber sensors for pressure. Since the development of such sensors is rather limited to date, the approach of this project is first of all exploratory with a theoretical basis and an increased understanding of the phenomena involved. The secondary aim of this work is to obtain the best possible performance (high resolution, large stroke, high sensitivity, and low measurement error).

2. THEORY

When a variety of environmental events are observed, pressure is an important measure. Precision applications and monitoring use many industrial processes with high precision. The fiber optic pressure sensor is well adapted for the usage with both human and animal bodies, making them useful for medical diagnosis. Body fluid pressure can be measured using PCF-based pressure sensors. Underwater pressure and temperature can be measured with these sensors [55].

The motivation for this paper is the first sensor developed based on PCF. New optical solutions are provided by PCFs; however, some of them are difficult to deal with. For example, the low optical transmission of PCF makes it difficult to use to make high-quality (low-loss, high-strength) splices and connectors [56]. It is strongly influenced by the condition of surrounding small holes [57].

The following equation for the refractive index of liquid water as a function of wavelength, temperature, and pressure was presented at the 9th International Conference on the Properties of Vapors, held in Munich, Germany, in 1979 [58]:

$$\begin{aligned} n(\lambda, T, P) \;=\; & \sqrt{\frac{a_1}{\lambda^2-\lambda_a^2} + a_2 + a_3\cdot\lambda^2 + a_4\cdot\lambda^4 + a_5\cdot\lambda^6} + \left(b_1 + b_2\cdot\lambda^2 + b_3\cdot\lambda^4\right)(T-T_b) \\ & + \left(b_4 + b_5\cdot\lambda^2 + b_6\cdot\lambda^4\right)\cdot(T-T_b)^2 + \left(b_7 + b_8\cdot\lambda^2 + b_9\cdot\lambda^4\right)\cdot(T-T_b)^3 \\ & + \left[c_1 + c_2\cdot\lambda^2 + \left(c_3 + c_4\cdot\lambda^2\right)\cdot T\right](P-P_b) + \left(c_5 + c_6\cdot\lambda^2\right)\cdot(P-P_b)^2 \end{aligned} \tag{1}$$

With the range of validity of:

$$0.182\,\mu\text{m} \leq \lambda \leq 2.770\,\mu\text{m}$$
$$-10°\text{C} \leq T < 100°\text{C}$$
$$1\,\text{bar} \leq P \leq 1200\,\text{bar}$$

The value of the coefficient in Eq. (1) is determined by the least squares method [44], and reference temperature $T_b = 20°\text{C}$ selected according to International Practical Temperature 1968 Scale corresponds to the temperature of $T_b = 19.993°\text{C}$ and reference pressure for $P_b = 1\,\text{atm} = 1.01325\,\text{bar}$, considering these conditions were used to make the majority of measurements. The numerical values of the coefficients are given in Table 1. Wavelength λ, temperature T, and pressure P must be given in µm, °C, and bar in Eq. (1) [44].

Table 1. Numerical values of the coefficients of Eq. (1) [44].

$\lambda_a^2 = 0.018058$	$b_1 = -8.454823 * 10^{-5}$	$c_1 = 8.419632 * 10^{-6}$
$a_1 = 5.743534 * 10^{-3}$	$b_2 = -2.787742 * 10^{-5}$	$c_2 = 1.941681 * 10^{-5}$
$a_2 = 1.769238$	$b_3 = 2.608176 * 10^{-6}$	$c_3 = -7.762524 * 10^{-8}$
$a_3 = -2.797222 * 10^{-2}$	$b_4 = -2.050176 * 10^{-6}$	$c_4 = 4.371257 * 10^{-8}$
$a_4 = 8.715348 * 10^{-3}$	$b_5 = 1.019989 * 10^{-6}$	$c_5 = 7.089664 * 10^{-9}$
$a_5 = -1.413942 * 10^{-3}$	$b_6 = -2.611919 * 10^{-6}$	$c_6 = -2.240384 * 10^{-8}$
	$b_7 = 8.194989 * 10^{-9}$	
	$b_8 = -8.107707 * 10^{-9}$	
	$b_9 = 4.877274 * 10^{-8}$	

Indeed, in this paper we intend to use a numerical method to study the chromatic dispersion of the proposed PCF. Sellmeier's equation (Eq. (2)) can be used to measure and model the effective refractive index n_{eff} of hollow airholes that have been set in silica as the background material, as stated by [59]:

$$n^2 - 1 = \frac{0.6961663 \cdot \lambda^2}{\lambda^2 + (0.0684043)^2} + \frac{0.4079426 \cdot \lambda^2}{\lambda^2 - (0.1162414)^2} + \frac{0.8974794 \cdot \lambda^2}{\lambda^2 - (9.896161)^2} \tag{2}$$

where λ is the operating wavelength. This equation will help to calculate the dispersion profile of the structure.

3. DESIGN OF PCF

A novel device was presented and developed using a numerical method. It consists of different sizes of the airholes that were chosen after multiple simulations to achieve a good curve in dispersion. It makes use of the fact that when a fluid is injected at an overhead pressure, the variation in hole size between the core and cladding causes a varied infusion speed inside the holes. The simulated PCF is shown in Fig. 3(c). It can be seen from this figure that the fiber structure has six rings and contains three sizes of airholes. In the first ring, the diameter of the airholes is $d_1 = 0.7\,\mu\text{m}$. In the second ring, the diameter is $d_2 = 1\,\mu\text{m}$, and the lattice pitch $\Lambda = 2.3\,\mu\text{m}$ and the remaining airholes are $d = 1.46\,\mu$ m. the PCF's background is silica, which is represented as the core and has a refractive index of 1.45 as highlighted in Fig. 3(a). We can find the specific parameter of our PCF in Table 2.

Figure 3(b) shows the profile index when injecting in the air-holes the selective analyte which is water.

Because of variations in the refractive index of water, which is sensitive to pressure, the airholes are filled with water since it contains a large part of the biochemical solution. In this work, we contribute by demonstrating how pressure impacts PCF dispersion. We will use liquid that penetrates air pores to show how pressure directly affects dispersion.

Table 2. The parameters of the proposal PCF.

Parameter	**Value (μm)**
Period Λ	2.3
Diameter d	1.46
Diameter d_1	0.7
Diameter d_2	1
Outer cladding diameter	125
Coating diameter	245

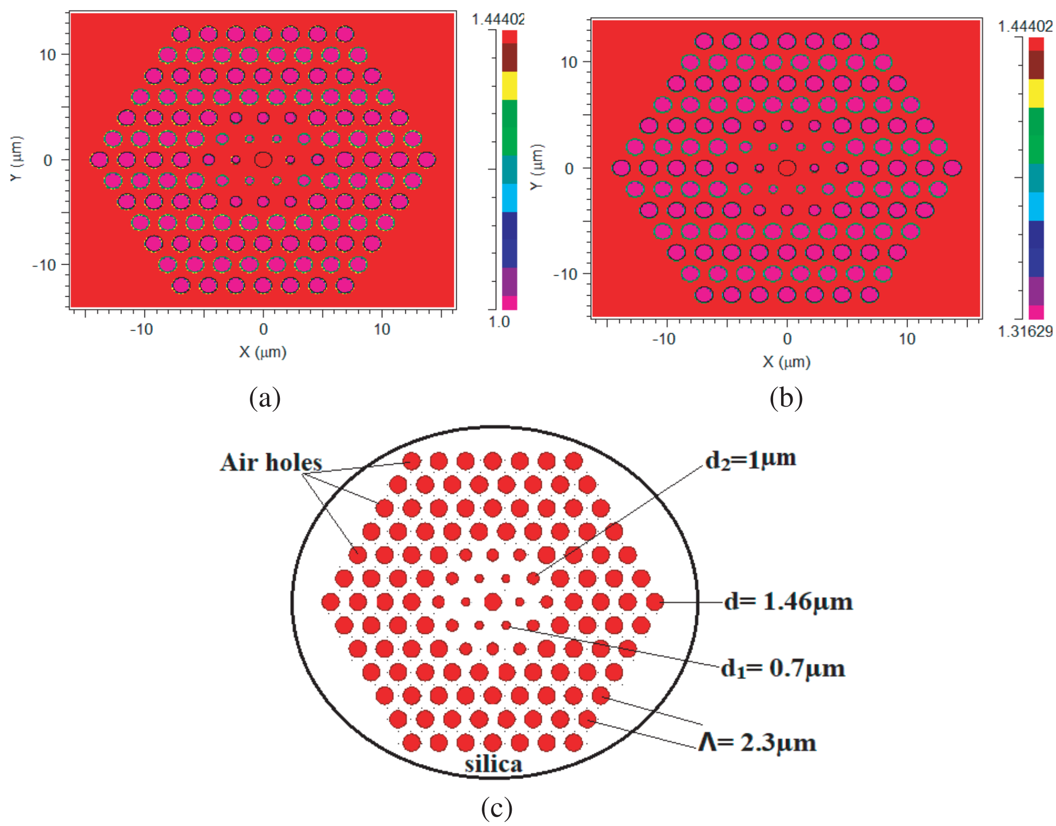

Figure 3. Proposal structure. (a) With airholes. (b) Holes infiltrating with water. (c) The PCF cross-section.

4. RESULTS AND DISCUSSION

Firstly, we will simulate the dispersion of the PCF by numerical method with and without water to study the differences and the influences of infiltrating water on PCF. From Fig. 4, we observe that when the holes of the PCF were filled with air, the zero-dispersion wavelength (ZDW) was located at a value of 1.16 μm. However, after filling water in the airholes, the ZDW was shifted to 1.4 μm. This is a good result in the location of the ZDW.

The refractive index of air-holes is largely independent of temperature and pressure, and we can conclude that the effect of the different pressure on the PCF is insignificant, and the refractive index of water (H_2O) is dependent on both temperature and pressure. For that reason, the air-holes were filled with water. The temperature was fixed at 25°C, and the pressure was chosen as 2 bar. The dispersion

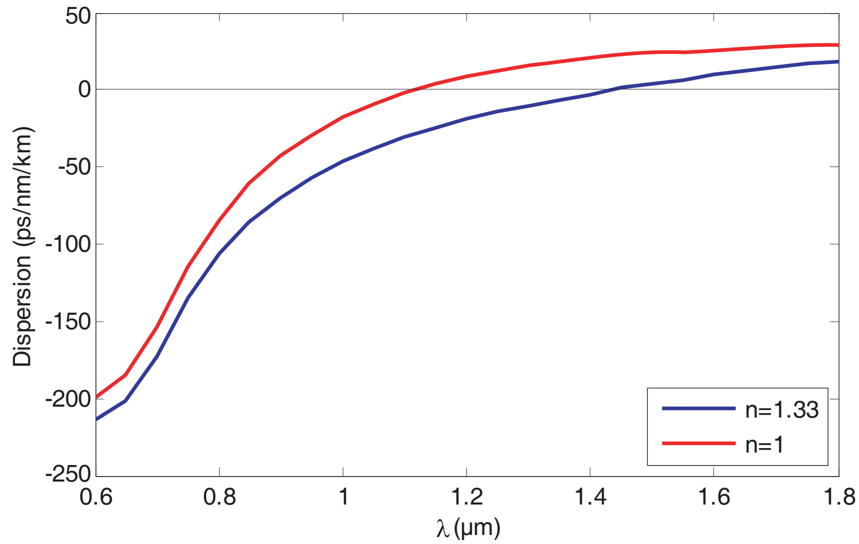

Figure 4. The variation of the chromatic dispersion with and without infiltrating air-holes with water.

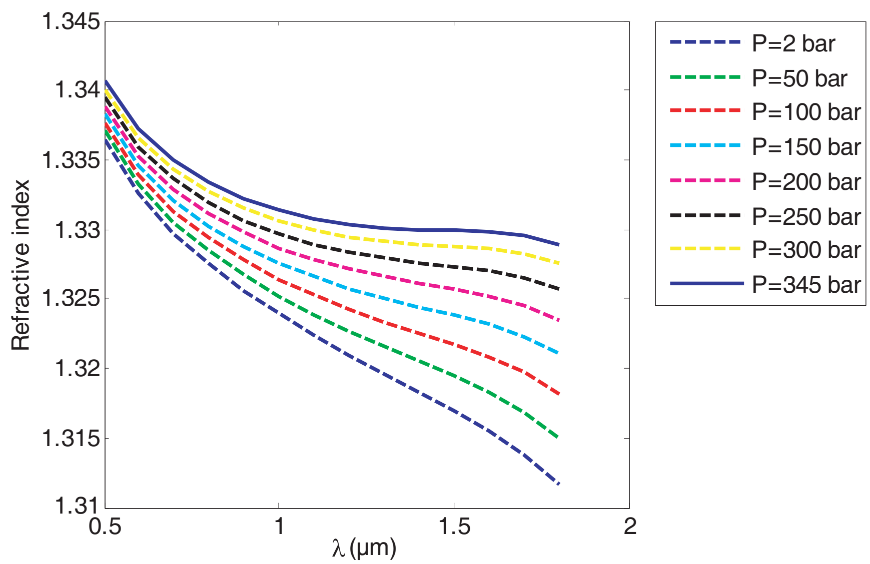

Figure 5. The refractive index of water as a function of wavelength for different pressure.

was moved to large wavelengths when holes were infiltrated with water. Chromatic dispersion is relative to the refractive index n (λ, T, P) and also relative to pressure effectively.

Figure 5 shows the change in the refractive index of water as a function of wavelength for various pressures. We notice that the pressure directly affects dispersion, and when the pressure increases, the refractive index increases.

The next step is to change the pressure. We start our simulation to calculate the dispersion of the PCF infiltrated with water for different pressure. The lower pressure was 2 bar, and the higher one was 345 bar. This range was chosen relative to [60]. Fig. 6 shows the relation of the shift in chromatic dispersion with the change of pressures, demonstrating that the PCF may be used as a pressure sensor. This change indicates the relationship between the chromatic dispersion and the pressure.

Then, we restart our simulation with a numerical method to calculate the variation of the dispersion of PCF infiltrating with water. At this stage, we will change the pressure to the range of 10 bar to

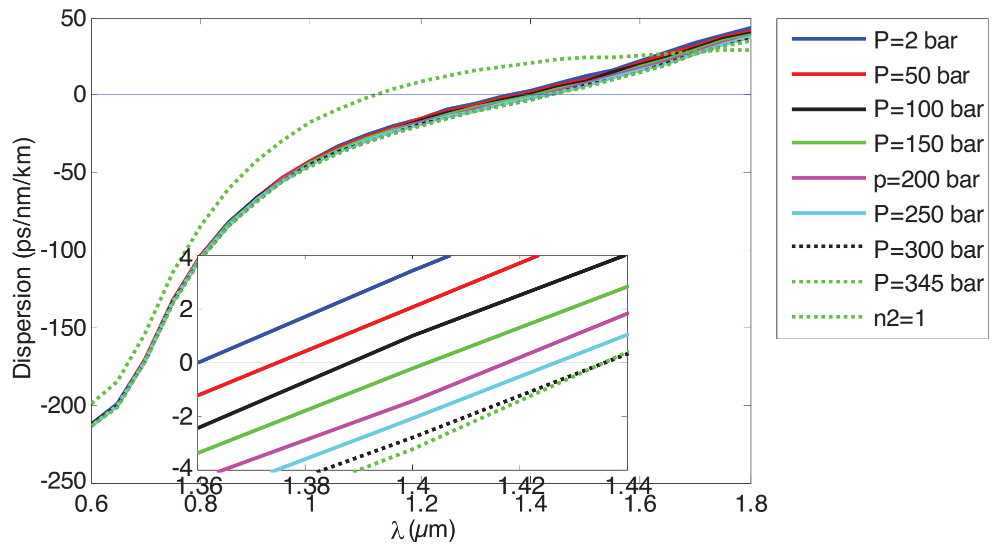

Figure 6. The variation of the chromatic dispersion at a different pressure.

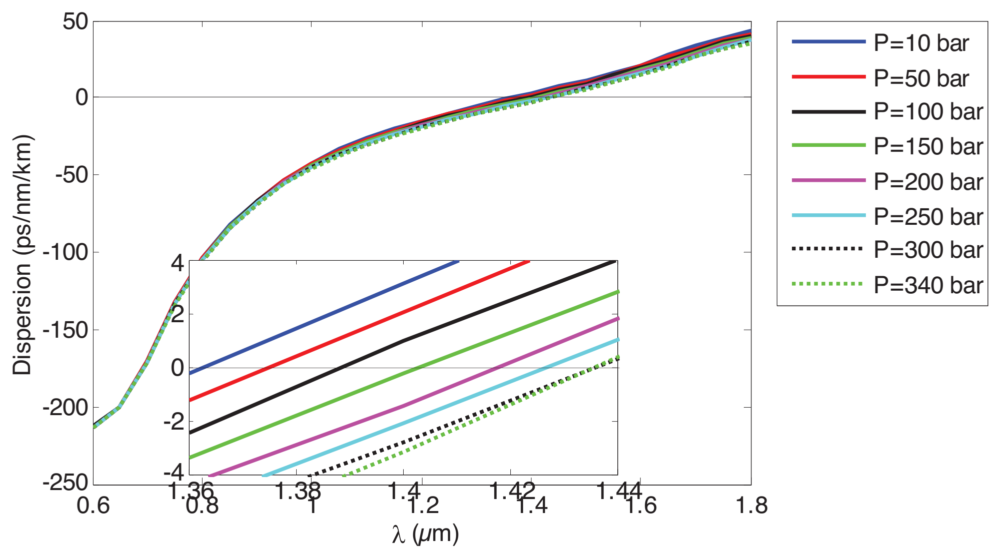

Figure 7. The chromatic dispersion as function of wavelength in different pressure.

340 bar. The shift during the change of the dispersion was recorded to evaluate the sensitivity of the sensor. Fig. 6 shows the dispersion as a function of wavelength by raising the pressure from 10 bar to 340 bar. Clearly from the curve illustrated in Fig. 7, there is a relation between the dispersion and the pressure. The dispersion is sensitively dependent on the pressure. The sensing property is analyzed by infiltrating water into the air-holes.

For computing the sensitivity of this pressure sensor, we will choose three different wavelengths, 1.1 μm, 1.4 μm, and 1.7 μm, and we will study the variation of chromatics dispersion at each of these wavelengths.

So firstly, measurements were made at the wavelength 1.1 μm. Fig. 8(a) shows the characteristic curve of the variation of chromatic dispersion at 1.1 μm. The sensitivity was calculated as: $S\,(\text{ps/nm/km})/\text{bar} = \Delta D/\Delta P$. It can be noticed from Fig. 8(b) that the simulation sensitivity of pressure is around 0.01 (ps/nm/km)/bar by using the quadratic fitting.

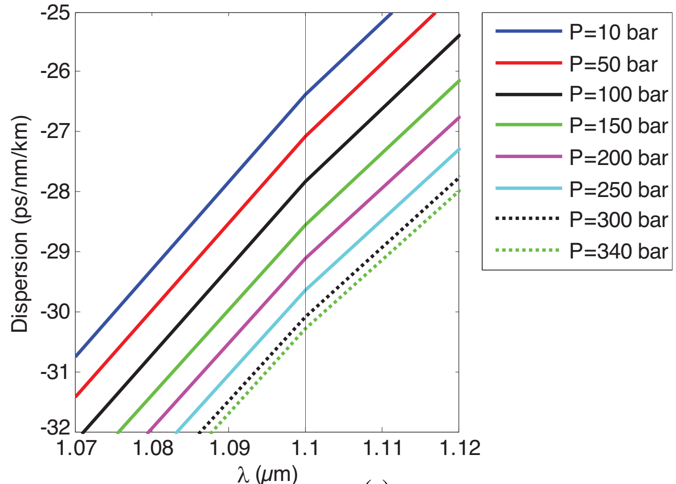

(a)

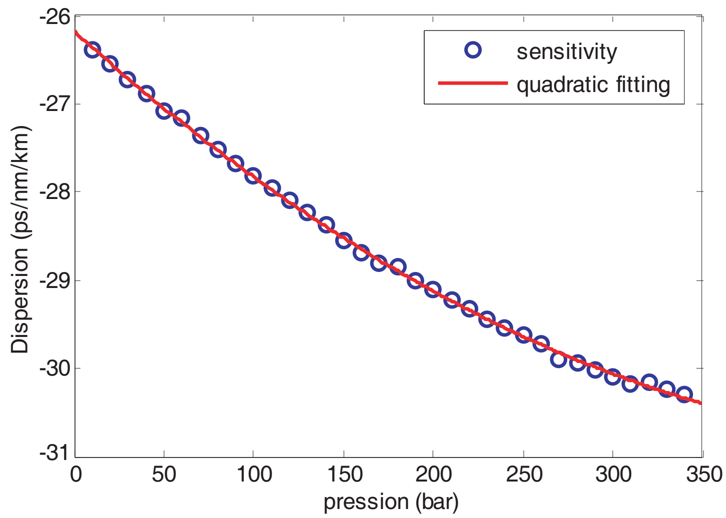

(b)

Figure 8. (a) Dispersion in the function of wavelength. (b) Dispersion in the function of pressure for the wavelength 1.1 µm.

Then, we use the case when the wavelength is 1.4 µm to calculate the sensitivity. Fig. 9(a) clarifies the variation of the chromatic dispersion when $\lambda = 1.4\,\mu$m, and the calculations were performed at a fixed wavelength (1.4 µm) and different levels of the applied pressure. We can calculate the sensitivity as shown in Fig. 9(b). According to the measured experimental data, the average value for the pressure sensitivity can be calculated to be -0.0207737 (ps/nm/km)/bar by applying the quadratic fitting.

Afterward, we will take the wavelength $\lambda = 1.7\,\mu$m as shown in Fig. 10(a) and calculate the average value of the sensitivity of the sensor. Fig. 10(b) illustrates the sensitivity when the wavelength was 1.7 µm. At this point and by using the quadratic fitting, we can calculate the sensor's sensitivity to be -0.0236908 (ps/nm/km)/bar.

After several calculations and comparisons among these wavelengths that have been chosen, it can be noticed that the sensitivity when the wavelength is 1.7 µm is better than the sensitivity when the wavelength is 1.1 and 1.4 µm. It can be seen from Fig. 11 that this pressure sensor is more sensitive to the rising of the wavelength.

The sensitivity changes with the change of wavelength. From this, it can be illustrated that there is a little change of sensitivity whereas a rapid change. Thus, it is possible to employ the suggested sensor for pressure sensing.

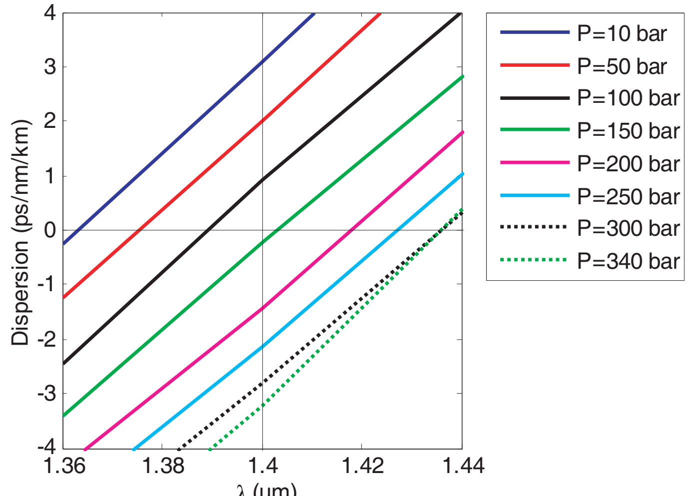

(a)

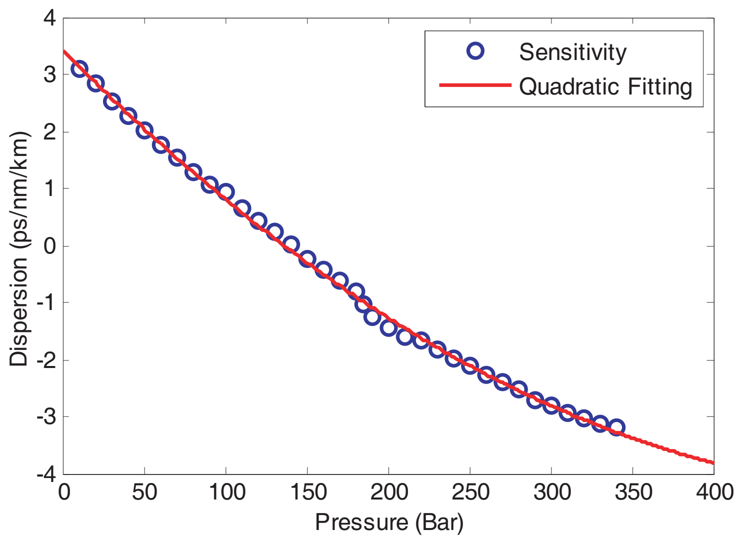

(b)

Figure 9. (a) Dispersion in the function of wavelength. (b) Dispersion in the function of pressure for the wavelength 1.4 μm.

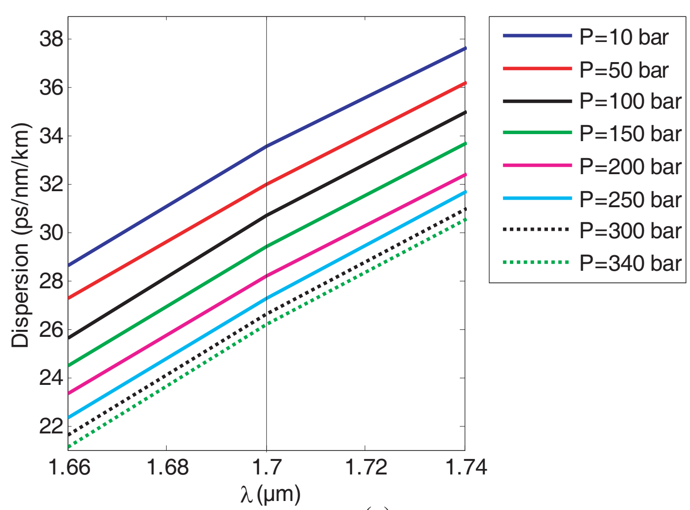

(a)

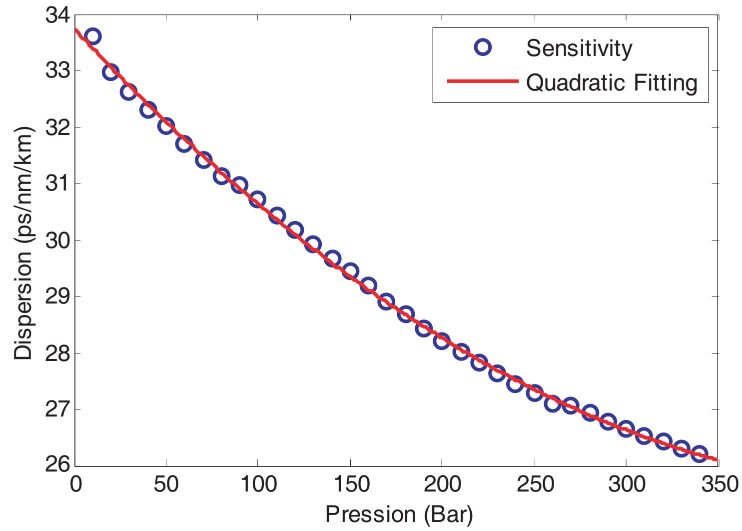

(b)

Figure 10. (a) Dispersion in the function of wavelength. (b) Dispersion in the function of pressure for the wavelength 1.7 μm.

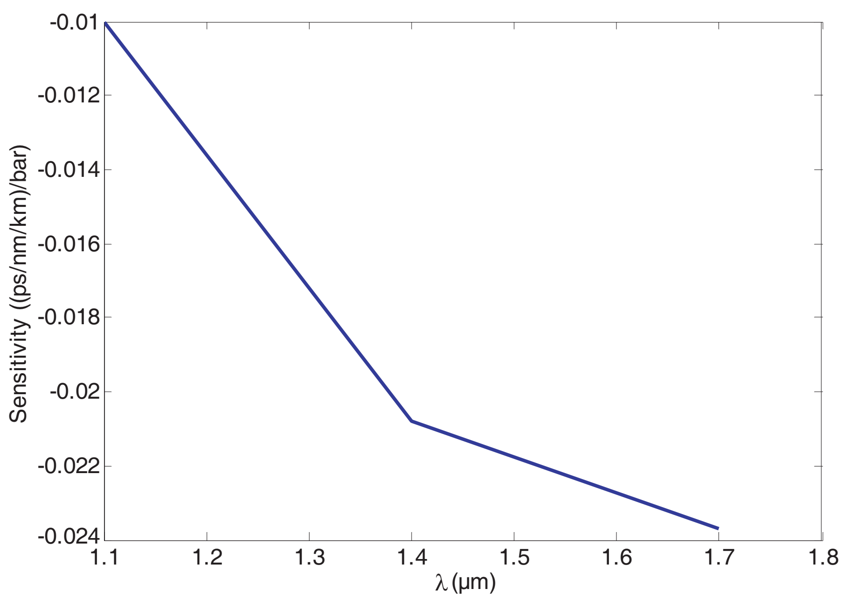

Figure 11. Sensitivity in function wavelength.

5. CONCLUSION

In this study, we have studied how pressure affected PCF's chromatic dispersion, by infiltrating the air-holes with water. Consequently, a successful PCF pressure sensor has been developed using a numerical method by infiltrating water in the air-holes. The results indicate that the pressure sensitivity is −0.01 (ps/nm/km)/bar −0.0207737 (ps/nm/km)/bar and −0.0236908 (ps/nm/km)/bar at the wavelengths 1.1 μm, 1.4 μm, and 1.7 μm, respectively. The sensitivity at 1.7 μm is the best. The sensor has been operating successfully. It has been shown that the more the wavelength increases, the more the sensor becomes sensitive. This sensor offers direct sensing, which is simple to design, small in size, and simple to manufacture, making it a perfect candidate for pressure sensitivity.

REFERENCES

1. Olyaee, S. and A. A. Dehghani, "High resolution and wide dynamic range pressure sensor based on two-dimensional photonic crystal," *Photonic Sensors*, Vol. 2, No. 1, 92–96, 2012.
2. Beravat, R., G. K. Wong, M. H. Frosz, X. M. Xi, and P. S. J. Russell, "Twist-induced guidance in coreless photonic crystal fiber: A helical channel for light," *Science Advances*, Vol. 2, No. 11, e1601421, 2016.
3. Abbaszadeh, A., S. Makouei, and S. Meshgini, "High sensitive triangular photonic crystal fiber sensor design applicable for gas detection," *Advanced Electromagnetics*, Vol. 10, No. 1, 1–5, 2021.
4. Sakib, M. N., S. R. Islam, T. V. Mahendiran, L. F. Abdulrazak, M. S. Islam, I. M. Mehedi, and M. B. Hossain, "Numerical study of circularly slotted highly sensitive plasmonic biosensor: A novel approach," *Results in Physics*, Vol. 17, 103130, 2020.
5. Upadhyay, A., S. Singh, D. Sharma, and S. A. Taya, "Analysis of proposed PCF with square air hole for revolutionary high birefringence and nonlinearity," *Photonics and Nanostructures — Fundamentals and Applications*, Vol. 43, 100896, 2021.
6. Islam, M., M. R. Islam, Z. Tasnim, R. Islam, R. L. Khan, and E. Moazzam, "Low-loss and dispersion-flattened octagonal porous core PCF for terahertz transmission applications," *Iranian Journal of Science and Technology, Transactions of Electrical Engineering*, Vol. 44, No. 4, 1583–1592, 2020.
7. Ferdous, A. I., M. S. Anower, and M. A. Habib, "A hybrid structured PCF for fuel adulteration detection in terahertz regime," *Sensing and Bio-Sensing Research*, Vol. 33, 100438, 2021.
8. Kumar, A., P. Verma, and P. Jindal, "Decagonal solid core PCF based refractive index sensor for blood cells detection in terahertz regime," *Optical and Quantum Electronics*, Vol. 53, No. 4, 1–13, 2021.
9. Lavanya, A. and G. Geetha, "A novel hybrid hexagonal photonic crystal fibre for optical fibre communication," *Optical Fiber Technology*, Vol. 59, 102321, 2020.
10. Vijayalakshmi, D., C. T. Manimegalai, and P. Selvakumar, "Bi-core photonic crystal fiber for blood component detection," *Journal of Optics*, 1–8, 2022.
11. Muduli, N., J. S. N. Achary, and H. K. Padhy, "Grade-2 Teflon (AF1601) PCF for optical communication using 2D FDTD technique: A simplest design," *Journal of Modern Optics*, Vol. 63, No. 7, 685–691, 2016.
12. Liu, H., B. Wu, C. Chen, B. Zhao, X. Zhang, and H. Zhang, "D-shaped tellurite photonic crystal fiber hydrogen and methane sensor based on four-wave mixing with SPR effect," *Photonic Sensors*, Vol. 13, No. 1, 1–15, 2023.
13. Rajesh, A., S. Chandru, and S. Robinson, "Investigation of defective hybrid cladding with silicon nanocrystal PCF for supercontinuum generation," *Laser Physics*, Vol. 31, No. 12, 126206, 2021.
14. Han, J., E. Liu, and J. Liu, "Circular gradient-diameter photonic crystal fiber with large mode area and low bending loss," *JOSA A*, Vol. 36, No. 4, 533–539, 2019.
15. Wang, Q., L. Kong, Y. Dang, F. Xia, Y. Zhang, Y. Zhao, and J. Li, "High sensitivity refractive index sensor based on splicing points tapered SMF-PCF-SMF structure Mach-Zehnder mode interferometer," *Sensors and Actuators B: Chemical*, Vol. 225, 213–220, 2016.
16. Paul, B. K., M. G. Moctader, K. Ahmed, and M. A. Khalek, "Nanoscale GaP strips based photonic crystal fiber with high nonlinearity and high numerical aperture for laser applications," *Results in Physics*, Vol. 10, 374–378, 2018.
17. Chandru, S., T. Shankar, and A. Rajesh, "Investigation on nanocore-centred nonlinear PCF for high nonlinearity and low dispersion," *Ceramics International*, Vol. 48, No. 11, 16042–16048, 2022.
18. Wang, E., Q. Han, X. Zhou, H. Yuan, and J. Li, "A bend-resistant photonic crystal fiber with large effective mode area," *Optical Fiber Technology*, Vol. 71, 102902, 2022.
19. Zhao, Q., J. Liu, H. Yang, H. Liu, G. Zeng, and B. Huang, "High birefringence D-shaped germanium-doped photonic crystal fiber sensor," *Micromachines*, Vol. 13, No. 6, 826, 2022.

20. Thi, T. N., D. H. Trong, and L. C. Van, "Supercontinuum generation in ultra-flattened near-zero dispersion PCF with C7H8 infiltration," *Optical and Quantum Electronics*, Vol. 55, No. 1, 1–22, 2023.
21. Wang, B., C. Jia, J. Yang, Z. Di, J. Yao, and J. Zhang, "Highly birefringent, low flattened dispersion photonic crystal fiber in the terahertz region," *IEEE Photonics Journal*, Vol. 13, No. 2, 1–10, 2021.
22. Asaduzzaman, S., H. Rehana, T. Bhuiyan, D. Sarma, O. S. Faragallah, M. Eid, and A. N. Z. Rashed, "Extremely high birefringent slotted core umbrella-shaped photonic crystal fiber in terahertz regime," *Applied Physics B*, Vol. 128, No. 8, 1–12, 2022.
23. Singla, S. and P. Singal, "Photonic crystal fiber: Construction, properties, developments and applications," *Int. J. Electron. Eng.*, Vol. 9, 1–8, 2017.
24. Zhao, Q., J. Qu, G. Peng, and C. Yu, "Endless single-mode Photonics Crystal Fiber Metalens for broadband and efficient focusing in near-infrared range," *Micromachines*, Vol. 12, No. 2, 219, 2021.
25. Zhao, F., H. Zhang, L. Wang, R. Ma, T. Xu, and N. Zhu, "A surrogate-assisted Jaya algorithm based on optimal directional guidance and historical learning mechanism," *Engineering Applications of Artificial Intelligence*, Vol. 111, 104775, 2022.
26. Hu, D. J. J., Z. Xu, and P. P. Shum, "Review on photonic crystal fibers with hybrid guiding mechanisms," *IEEE Access*, Vol. 7, 67469–67482, 2019.
27. Ayyanar, N., D. Vigneswaran, M. Sharma, M. Sumathi, M. M. Rajan, and S. Konar, "Hydrostatic pressure sensor using high birefringence photonic crystal fibers," *IEEE Sensors Journal*, Vol. 17, No. 3, 650–656, 2016.
28. Dudley, J. M., G. Genty, A. Mussot, A. Chabchoub, and F. Dias, "Rogue waves and analogies in optics and oceanography," *Nature Reviews Physics*, Vol. 1, No. 11, 675–689, 2019.
29. Leal-Junior, A., C. Díaz, A. Frizera, H. Lee, K. Nakamura, Y. Mizuno, and C. Marques, "Highly sensitive fiber-optic intrinsic electromagnetic field sensing," *Advanced Photonics Research*, Vol. 2, No. 1, 2000078, 2021.
30. Verma, R. K., P. Suwalka, and J. Yadav, "Detection of adulteration in diesel and petrol by kerosene using SPR based fiber optic technique," *Optical Fiber Technology*, Vol. 43, 95–100, 2018.
31. Dalla Vedova, M. D. L., P. C. Berri, P. Maggiore, and G. Quattrocchi, "Design and development of innovative FBG-based fiber optic sensors for aerospace applications," *Journal of Physics: Conference Series*, Vol. 1589, No. 1, 012012, IOP Publishing, Jul. 2020.
32. Hyer, H. C., D. C. Sweeney, and C. M. Petrie, "Functional fiber-optic sensors embedded in stainless steel components using ultrasonic additive manufacturing for distributed temperature and strain measurements," *Additive Manufacturing*, Vol. 52, 102681, 2022.
33. Yang, L., F. Wei, J. M. Liu, and S. Wang, "Functional hybrid micro/nanoentities promote agro-food safety inspection," *Journal of Agricultural and Food Chemistry*, Vol. 69, No. 42, 12402–12417, 2021.
34. Yao, Y., M. Yan, and Y. Bao, "Measurement of cable forces for automated monitoring of engineering structures using fiber optic sensors: A review," *Automation in Construction*, Vol. 126, 103687, 2021.
35. Habel, W. R., "Guidelines and standards for fiber optic sensors: Quo vadis?," *Smart Structures and Materials 2006: Smart Sensor Monitoring Systems and Applications*, Vol. 6167, 339–347, SPIE, Mar. 2006.
36. Xuan, K. D., L. C. Van, V. C. Long, Q. H. Dinh, L. Van Mai, M. Trippenbach, and R. Buczyński, "Influence of temperature on dispersion properties of photonic crystal fibers infiltrated with water," *Optical and Quantum Electronics*, Vol. 49, No. 2, 1–12, 2017.
37. Frazao, O., J. L. Santos, F. M. Araujo, and L. A. Ferreira, "Optical sensing with photonic crystal fibers," *Laser & Photonics Reviews*, Vol. 2, No. 6, 449–459, 2008.
38. Jin, W., L. M. Xiao, K. S. Hong, and Y. B. Liao, "Novel devices and sensors based on microstructured optical fibers," *Advanced Sensor Systems and Applications III*, Vol. 6830, 476–485, SPIE, Jan. 2008.
39. Michie, A., J. Canning, K. Lyytikäinen, M. ˚ Aslund, and J. Digweed, "Temperature independent highly birefringent photonic crystal fibre," *Optics Express*, Vol. 12, No. 21, 5160–5165, 2004.

40. Srivastava, R., Y. K. Prajapati, S. Pal, and S. Kumar, "Micro-channel plasmon sensor based on a D-shaped photonic crystal fiber for malaria diagnosis with improved performance," *IEEE Sensors Journal*, Vol. 22, No. 15, 14834–14841, 2022.
41. Boufenar, R., M. Bouamar, and A. Hocini, "Numerical analysis of a temperature sensor based on the photonic band gap effect in a photonic crystal fiber," *Chinese Journal of Physics*, Vol. 56, No. 3, 1126–1132, 2018.
42. Bock, W. J., J. Chen, T. Eftimov, and W. Urbanczyk, "A photonic crystal fiber sensor for pressure measurements," *IEEE Transactions on Instrumentation and Measurement*, Vol. 55, No. 4, 1119–1123, 2006.
43. Mathews, S., Y. Semenova, and G. Rajan, "Liquid crystal optical fibers for sensing applications," *Optical Fiber Sensors: Advanced Techniques and Applications*, 151–179, CRC Press, 2015.
44. Lou, Z., L. Wang, and G. Shen, "Recent advances in smart wearable sensing systems," *Advanced Materials Technologies*, Vol. 3, No. 12, 1800444, 2018.
45. Liu, H., D. W. Miller, and J. Talnagi, "Gamma radiation resistant Fabry-Perot fiber optic sensors," *Review of Scientific Instruments*, Vol. 73, No. 8, 3112–3118, 2002.
46. Wu, J., K. L. Deng, R. Guida, and B. K. Lee, "Fiber-optic photo-acoustic spectroscopy sensor for harsh environment gas detection," *Photonic Fiber and Crystal Devices: Advances in Materials and Innovations in Device Applications*, Vol. 6698, 93–99, SPIE, Sep. 2007.
47. Rahim, A., A. Hermans, B. Wohlfeil, D. Petousi, B. Kuyken, D. Van Thourhout, and R. G. Baets, "Taking silicon photonics modulators to a higher performance level: State-of-the-art and a review of new technologies," *Advanced Photonics*, Vol. 3, No. 2, 024003, 2021.
48. Essiambre, R. J., G. Kramer, P. J. Winzer, G. J. Foschini, and B. Goebel, "Capacity limits of optical fiber networks," *Journal of Lightwave Technology*, Vol. 28, No. 4, 662–701, 2010.
49. Shin, W., G. Jung, S. Hong, Y. Jeong, J. Park, D. Jang, and J. H. Lee, "Low frequency noise characteristics of resistor-and Si MOSFET-type gas sensors fabricated on the same Si wafer with In_2O_3 sensing layer," *Sensors and Actuators B: Chemical*, Vol. 318, 128087, 2020.
50. Padidar, S., V. Ahmadi, and M. Ebnali-Heidari, "Design of high sensitive pressure and temperature sensor using photonic crystal fiber for downhole application," *IEEE Photonics Journal*, Vol. 4, No. 5, 1590–1599, 2012.
51. Fu, H. Y., H. Y. Tam, L. Y. Shao, X. Dong, P. K. A. Wai, C. Lu, and S. K. Khijwania, "Pressure sensor realized with polarization-maintaining photonic crystal fiber-based Sagnac interferometer," *Applied Optics*, Vol. 47, No. 15, 2835–2839, 2008.
52. Zhong, X., Y. Wang, C. Liao, S. Liu, J. Tang, and Q. Wang, "Temperature-insensitivity gas pressure sensor based on inflated long period fiber grating inscribed in photonic crystal fiber," *Optics Letters*, Vol. 40, No. 8, 1791–1794, 2015.
53. Fu, H. Y., C. Wu, M. L. V. Tse, L. Zhang, K. C. D. Cheng, H. Y. Tam, and C. Lu, "High pressure sensor based on photonic crystal fiber for downhole application," *Applied Optics*, Vol. 49, No. 14, 2639–2643, 2010.
54. Bock, W. J., J. Chen, P. Mikulic, and T. Eftimov, "A novel fiber-optic tapered long-period grating sensor for pressure monitoring," *IEEE Transactions on Instrumentation and Measurement*, Vol. 56, No. 4, 1176–1180, 2007.
55. De, M., T. K. Gangopadhyay, and V. K. Singh, "Prospects of photonic crystal fiber as physical sensor: An overview," *Sensors*, Vol. 19, No. 3, 464, 2019.
56. Fortin, V., Y. O. Aydin, M. Bernier, R. Vallée, M. Rochette, F. Chenard, and J. S. Sanghera, "Post-processing soft glass optical fibers," *Mid-Infrared Fiber Photonics*, 233–302, Woodhead Publishing, 2022.
57. Chenard, F., O. Alvarez, E. Schartner, and H. Ebendorff-Heidepriem, "Mid-infrared chalcogenide polarization-maintaining single-mode fiber," *Optical Components and Materials XIX*, Vol. 11997, 109–121, SPIE, Mar. 2022.

58. Thormählen, I., J. Straub, and U. Grigull, "Refractive index of water and its dependence on wavelength, temperature, and density," *Journal of Physical and Chemical Reference Data*, Vol. 14, No. 4, 933–945, 1985.
59. Akowuah, E. K., T. Gorman, H. Ademgil, S. Haxha, G. K. Robinson, and J. V. Oliver, "Numerical analysis of a photonic crystal fiber for biosensing applications," *IEEE Journal of Quantum Electronics*, Vol. 48, No. 11, 1403–1410, 2012.
60. Sadeghi, J., H. Latifi, J. L. Santos, Z. Chenari, and F. Ziaee, "Behavior of a hollow core photonic crystal fiber under high radial pressure for downhole application," *Applied Physics Letters*, Vol. 104, No. 7, 071910, 2014.